ChemComm

COMMUNICATION

View Article Online
View Journal | View Issue

Cite this: *Chem. Commun.*, 2025, **61**, 5134

Received 4th December 2024,
Accepted 5th March 2025

DOI: 10.1039/d4cc06418f

rsc.li/chemcomm

Towards high-temperature fuel cells using sulfonated-phosphonated poly(pentafluorostyrene)†

Theresa Stigler, *[ab] Sebastian Auffarth, [ab] Maximilian Wagner,[ac] Andreas Hutzler, [a] Simon Thiele [ab] and Jochen Kerres *[ad]

Herein, we present a hybrid polymer material with phosphonic acid and sulfonic acid moieties on a poly(pentafluorostyrene) backbone utilizing the S_NAr Michaelis–Arbuzov and the *para*-fluoro-thiol reaction. Blending the hybrid material with a benzimidazole polymer yielded a mechanically stable membrane featuring proton conductivities up to three times higher than conventional Nafion N211 at temperatures above 120 °C.

Proton exchange membrane (PEM) materials have recently gained significant attention because of their applications in water electrolyzers, CO_2 reduction, and fuel cell technologies.[1,2] Their unique properties, including high proton conductivity and chemical stability, make them an attractive material for various industrial energy conversion applications.[3,4] The production of mechanically robust and highly conductive PEMs is of great importance for the high temperature PEM fuel cell technology (HT-PEMFC). Operating these fuel cell systems at high temperatures (120–170 °C) has several advantages, including higher tolerance of impure fuel streams, improved cathode kinetics, and a less complex water management.[5] These advantages of HT-PEMFC position it as a superior option compared to alternative fuel cell types, such as sugar-based fuel cells.[6] However, developing polyelectrolyte materials that function reliably between 120 °C and 170 °C is demanding. The state-of-the-art material Nafion lacks severe disadvantages in this temperature range due to a low glass transition temperature (~140 °C),[7,8] where the polymer chain partially softens. Furthermore, the proton conduction of sulfonated derivates relies on high humidification.[9] Hereby, water promotes the dissociation of protons from the sulfonic acid units and provides mobile hydrated protons. Polybenzimidazole membranes doped with phosphoric acid are attracting attention for their use in HT-PEMFC applications.[10,11] However, the main problem with these materials is the retention of phosphoric acids within the membrane.[12] In this study, enhanced proton conductivity at temperatures above 120 °C is addressed with a polymer material comprising both phosphonic acid and sulfonic acid groups, herein named hybrid material. The two different acid segments conduct protons in a cooperative manner at high and, hence, at anhydrous conditions.[13–16] The disadvantage of the sulfonated unit's inability to conduct at high temperatures is utilized as a proton donating counterpart to the phosphonated unit, thus assisting in establishing a combined mechanism for proton conduction. This complementary interaction between the two ionic groups effectively mitigates the limitations of both systems, offering the hybrid material significant potential for the use in HT-PEMFC applications. In fact, its performance surpasses that of the state-of-the-art material Nafion, showcasing its superior properties. Since the acidic moieties are covalently bound to the polymer structure, leakage of molecules is avoided. Furthermore, by blending the hybrid material with poly[2,2′-(*p*-oxydiphenylene)-5,5′-bibenzimidazole] (OPBI) an acid–base interaction is formed, thereby increasing the membrane's mechanical stability.

The free-radical polymerization of poly(pentafluorostyrene) (PPFS) was reported in a previous study.[17] The post-polymerization modification of PPFS using the Michaelis–Arbuzov and *para*-fluoro-thiol reaction enables precise control over the phosphonation[18,19] and sulfonation[17,20] ratios. At first, PPFS was substituted to a degree of 40% (PWN40), to achieve an optimal trade-off between membrane mechanical stability and proton conductivity.[21] Afterwards, thioalkylation under mild reaction conditions introduced chains terminated with sulfonic acid groups (PWN40-S). This method allows for precise control over the substitution degree and preserves the number of sulfonic acids by preventing side reactions such as

[a] *Forschungszentrum Jülich GmbH, Helmholtz Institute Erlangen-Nürnberg for Renewable Energy (IET-2), Cauerstr. 1, 91058 Erlangen, Germany. E-mail: th.stigler@fz-juelich.de, j.kerres@fz-juelich.de*
[b] *Department of Chemical and Biological Engineering, Friedrich-Alexander-Universität Erlangen-Nürnberg, Immerwahrstr. 2a, 91058 Erlangen, Germany*
[c] *Fraunhofer-Institut für Keramische Technologien und Systeme IKTS, Äußere Nürnberger Straße 62, 91301 Forchheim, Germany*
[d] *Chemical Resource Beneficiation Faculty of Natural Sciences, North-West University, Potchefstroom 2520, South Africa*

† Electronic supplementary information (ESI) available: Experimental section, polymer and membrane characterization. See DOI: https://doi.org/10.1039/d4cc06418f

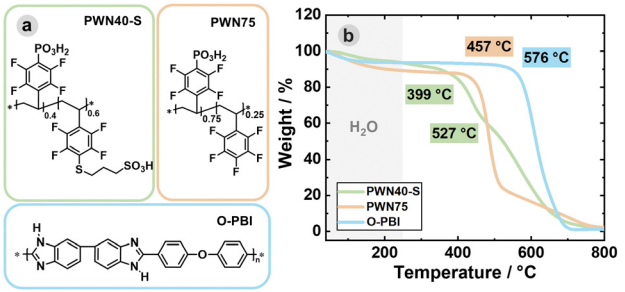

Fig. 1 (a) Chemical structures of PWN40-S, PWN75 and OPBI. (b) Thermogravimetric analysis of the pristine polymers with the assigned onset decomposition temperatures (heating rate: 10 K min^{-1}, carrier gas: synthetic air).

crosslinking.[22] The use of ^{19}F-NMR allowed for precise monitoring of the degree of functionalization for both reactions (see Fig. S1, ESI†). Furthermore, the characteristic peaks of the phosphonation and sulfonation were observed in the FT-IR spectroscopy, providing evidence of the successful incorporation of the acid groups (see Fig. S2, ESI†). As a reference material, PPFS with a phosphonation degree of 75% was synthesized, referred as PWN75. From thermogravimetric analysis measurements, the decomposition temperature of the polymers was determined. In Fig. 1, the thermogravimetric profiles are depicted with the respective decomposition temperatures and chemical structures. PWN40-S decomposes at a temperature of 399 °C, whereas the first degradation step can be referred to the cleavage of the $C_{aromatic}$–S bond of the alkyl side chain. Afterwards, the backbone and the phosphonic acid derivatives are decomposed (T = 527 °C). The decomposition profile aligns with previous studies.[17] Differential scanning calorimetry measurements shows no discernible glass transition temperature for PWN40-S (see Fig. S3, ESI†). Since OPBI has a glass transition temperature above 400 °C[23] the occurrence of a rubbery state within the operating temperature range of 120 °C to 170 °C can be excluded. The high thermal stability of the polymers, combined with their ability to maintain a glassy state, make them well-suited for fuel cell technologies operating within this temperature range. Ionically crosslinking for PWN40-S and PWN75 membranes was achieved by blending the acidic polymers with the basic polybenzimidazole OPBI. We assume that mainly ionic interaction occurs between the phosphonic acid moieties and the imidazole group of the OPBI, as the phosphonic acid units have a lower pK_a value compared to the sulfonic acid moieties. The pK_a values, calculated using ACD/pK_a DB software, are 0.5 ± 0.4 for phosphonic acid and 1.6 ± 0.5 for sulfonic acid moieties. A crucial consideration for membranes in HT-PEMFCs is their resistance to oxygen radical species. Therefore, we performed Fenton's tests at 80 °C. The mass loss of the PWN40-S + OPBI membrane was measured to be 0.11 ± 0.06% after 2 hours and 1.07 ± 0.81% after 6 hours. Notably, analysis of the Fenton's solution revealed a sharp fluorine signal, which we refer to HF (see Fig. S13, ESI†). Furthermore, proton conductivity measurements at room temperature showed a slight decline in proton conductivity after 6 hours, suggesting some degradation of the membrane's conductive properties (see Table S2, ESI†). Nevertheless, the membranes did not fully degrade within the test time, and films remained intact afterward. Besides oxidative stability, the mechanical resilience of the blend membranes was analyzed at room temperature at a relative humidity of 23 ± 1%. PWN40-S blended with 18 wt% OPBI shows a tensile strength of 44.5 ± 9.5 MPa and an elongation at break of 11.5 ± 3.7%, while PWN75 (OPBI content of 32 wt%) exhibits a tensile strength of 50.4 ± 4.1 MPa and an elongation at break of 8.5 ± 1.2% (see Fig. S6, ESI†).The pure OPBI membrane has a tensile strength of 58.6 ± 18 MPa and an elongation at break of 7.1 ± 3.3%. Overall, with increased OPBI content of the tested membranes, the tensile strength is increased and the elongation at break is decreased.

Another factor contributing to better elongation properties of the blend membrane with PWN40-S is attributed to the small aliphatic spacer between the PPFS backbone and the sulfuric acid units of the PWN40-S polymer, leading to enhanced mobility of the polymer segments.[24–26] In contrast, the reference blend membrane PWN75 shows strong ionic interactions without flexible moieties resulting in a restriction of stretching the polymer backbone and inducing strain during extension. We conclude that the mechanical strength of the synthesized polymer structure can be enhanced not only through blending but also by incorporating flexible aliphatic side chains.[17] The nanostructure of ionomers significantly influences their proton and water transport properties, which are ultimately the most critical factors for reliable fuel cell applications.[21,27] Therefore, the nanostructure of Ba^{2+} stained PWN40-S blend membrane was examined *via* high-angle angular dark-field scanning transmission electron microscopy (HAADF-STEM). Hereby, the polar acidic PWN40-S units, which do not engage in ionic crosslinking with the basic OPBI, absorb Ba^{2+} ions by an ion-exchange. The presence of the heavy Ba^{2+} ions enhances elastic scattering, causing the polar acidic segments to appear brighter in the HAADF signal compared to the nonpolar regions (see Fig. 2). Additional energy-dispersive X-ray (EDX) spectrum imaging of the cross-section reveals superimposed fluorine signals located in the polar segments. A comparison of the PWN40-S blend membrane with the reference membrane (PWN75 + OPBI, see Fig. S8, ESI†) shows that the PWN40-S blend membrane exhibits larger domain sizes (domain size PWN40-S ∼ 28.6 nm *versus* domain size PWN75 ∼ 2.2 nm). This indicates that the domains of the blend membrane PWN40-S are more broadly aligned, likely due to the sulfonic acid being attached *via* an aliphatic linker rather than directly to the perfluorinated ring. The difference in domain size is also reflected in the results of the Brunauer–Emmett–Teller (BET) surface analysis (see Fig. S5, ESI†).

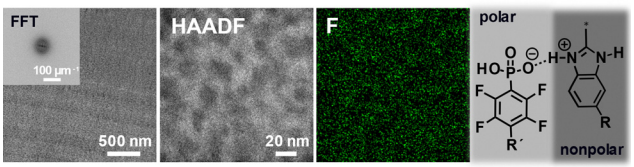

Fig. 2 Nanostructure analysis of PWN40-S blend membrane cross-section stained with Ba^{2+}. HAADF-STEM images and diffractogram for nanostructure size determination with corresponding fluorine EDX spectrum and simplified chemical structure with crosslinking and assignment of polar and nonpolar segments.

The PWN40-S + OPBI membrane shows a surface area of 19.9 $m^2\ g^{-1}$, whereas the PWN75 + OPBI membrane exhibits a larger surface area of 31.0 $m^2\ g^{-1}$. Based on these findings, we infer that a higher surface area is associated with a smaller average domain size. Overall, a clear distinction between polar and non-polar domains is evident in the PWN40-S blend membrane, which is considered to improve proton conductivity by focusing ion-conducting groups into nanochannels, thereby facilitating the formation of well-defined ion transport pathways.[19]

The water uptake and the proton conductivity of the blend membranes were investigated to obtain detailed information if the hybrid material is suitable for PEMFC application (Fig. 3). As expected, the trend applies that an increased water uptake enhances the proton conductivity (PWN75 < PWN40-S). In general, dimensional swelling and the formation of broader proton conductive channels are related to water absorption. Herein, the PWN40-S membrane gravimetrically absorbs approximately three times more water than the PWN75 blend membrane (see Fig. 3c). However, the volume swelling (swelling in width and length) of the hybrid membrane is only slightly higher than the reference membrane (10.8 ± 2.5% for PWN40-S and 6.8 ± 0.7% for PWN75 blend membrane). This difference may be attributed to the varying domain sizes of the two blend membranes. PWN40-s exhibits a larger domain size (28.6 nm), whereas PWN75 shows a smaller domain size of 2.2 nm. Herein, larger domains in the PWN40-S membrane can absorb more water without significant expansion in width and length. This suggests a further hypothesis: the nonpolar segments of the PWN40-S allow increased compressibility, reducing volume swelling despite higher water uptake. Enabling greater compression highlights the previously noted, more flexible polymer structure of PWN40-S.[28] Both membranes were blended to achieve the same IEC_{total} (3.0 meq. g^{-1}), yet the proton conductivity measured at room temperature with 0.5 M H_2SO_4 is markedly higher for the blend membrane PWN40-S ($\sigma_{PWN40\text{-}S}$ = 69.9 ± 8.1 mS cm^{-1}) compared to the blend membrane PWN75 (σ_{PWN75} = 2.7 ± 0.7 mS cm^{-1}). A possible explanation, namely the cooperative proton conduction of the hybrid materials, is discussed in the following.

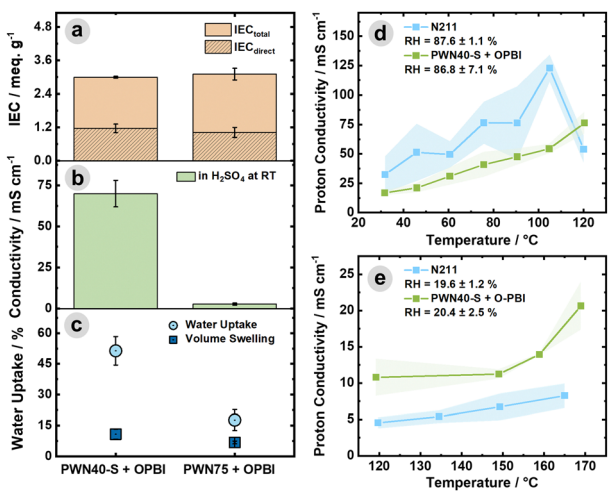

Fig. 3 (a) IEC_{total} and IEC_{direct}, (b) proton conductivity at room temperature in 0.5 M H_2SO_4, and (c) water uptake (gravimetric) and volume swelling after 1 day at 85 °C of PWN40-S + OPBI and PWN75 + OPBI. Proton conductivity of N211 and the PWN40-S OPBI blend membrane (d) at a temperature range from 30 °C to 120 °C with high relative humidity level, (e) at elevated temperature ranging from 120 °C to 170 °C with anhydrous conditions.

To compare the hybrid polymer with state-of-the-art polymer material, temperature dependent through-plane conductivity measurements were performed with a Nafion 211 (N211) membrane. At the low temperature range from 30 °C to 120 °C with high relative humidity (around 87%), the N211 membrane shows a better proton conductivity than the in-house made hybrid blend membrane. However, at a temperature of 120 °C the N211 membrane exhibits a noticeable decline in conductivity (σ = 54.0 ± 11.5 mS cm^{-1}), whereas the PWN40-S membrane exhibits an enhanced conductivity of 76.3 ± 9.3 mS cm^{-1}. At a low relative humidity level of about 20%, the hybrid membrane outperforms the N211 membrane in the high temperature range (120–170 °C). These results confirm the well-known limitations of Nafion, including its restricted application temperature range due to its dependence on hydration for proton conduction.[29–31] The analysis of the activation energy (E_a) provides insights into the proton conduction mechanism (see Fig. S10, ESI†). In general, a lower Ea corresponds to easier proton conduction within the membrane, facilitating faster proton transport.[32] At temperatures between 30–100 °C and relative humidity of approximately 87%, the N211 membrane exhibits an E_a of 14.4 ± 0.8 kJ mol^{-1} (see Table S2, ESI†). This suggests a proton conductivity based on a hopping mechanism, which is more dominant at high water content.[33,34] At elevated temperatures (120–170 °C) and low relative humidity (20%), N211 displays an E_a of 19.4 ± 1.1 kJ mol^{-1}, consistent with previously reported values.[35] In contrast, the PWN40-S + OPBI blend membrane shows an E_a of 32.7 ± 0.9 kJ mol^{-1} between 30–75 °C (87%RH), whereas at higher temperatures (75–100 °C) at the same relative humidity, the Ea decreases to 9.0 ± 0.5 kJ mol^{-1}. Notably, within the temperature range of 120–150 °C and low relative humidity (20%), the PWN40-S + OPBI membrane exhibits a significantly lower E_a of 5.4 ± 1.9 kJ mol^{-1}, indicating a relatively low energy barrier for proton conduction. We relate this behaviour to the cooperative conduction of sulfonic and phosphonic acid groups, where sulfonic acid units act as proton donors to the phosphonated units, facilitating a combined proton conduction mechanism. As a result, this interaction enhances proton conductivity compared to the reference membrane, N211. However, at temperatures exceeding 150 °C, the Ea rises sharply to 40.3 ± 7.0 kJ mol^{-1}, suggesting a shift in the proton conduction mechanism. Based on these findings, we propose that the optimal operating temperature range for the PWN40-S + OPBI membrane is between 100 °C and 150 °C. This range bridges the gap between LT and HT operations, offering a promising solution for applications requiring efficient proton conduction within this temperature window. In addition, temperature-dependent conductivity measurements of the reference membrane PWN75 + OPBI could not be performed due to its diminished conductivity, showing ultimately that improved proton conduction can be achieved by a combined ionic acid system. To confirm that no

acid moieties leach from the membrane and thus reduce proton conductivity, a long-term conductivity test was performed at 120 °C for 50 hours. Only minor variations in proton conductivity (47.7 ± 3.2 mS cm^{-1}) were observed, which may also be caused by fluctuations in humidity (see Fig. S11, ESI†). This result is in good agreement with a stability test in an aqueous environment. Membrane pieces were immersed in 10 wt% H_2SO_4 solution at 85 °C for 504 h. A mass loss of 6.1 ± 0.4% for the PWN40-S blend membrane is observed. Herein, the minor mass loss might be attributed to weighing inaccuracies or dissolution of solvent residues in the membrane. The investigation of the sulfuric acid solution after the treatment *via* NMR reveals no polymer peaks, verifying the retention of water-soluble acidic polymer units *via* electrostatic interactions with basic moieties of OPBI.

To conclude, the temperature-dependent conductivity test and subsequent analysis of the activation energy reveal a distinct difference in proton conduction behaviour compared to N211, particularly above 100 °C at anhydrous conditions. This suggests a cooperative conduction mechanism between the phosphonic acid and sulfonic acid units, which is further supported by the improved performance observed at these elevated temperatures. These results strongly emphasize the usage of hybrid membranes in HT-PEMFCs, closing the gap between low temperature and high temperature PEM applications. Further approaches can use these results as a blueprint and enhance the general membrane properties by adjusting the sulfonic acid and phosphonic acid units in terms of the length of the aliphatic chain, ratio, and finally, the blend ratio with OPBI.

Writing – original draft: T. St.; methodology: T. St.; data curation: T. St.; investigation: T. St., A. H.; conceptualization: T. St., S. A., M. W.; visualization: T. St., S. A.; writing – review and editing: S. A., M. W., A. H., S. T., J. K.; supervision: S. T., J. K.; funding acquisition: S. T., J. K.

The authors thankfully acknowledge the funding from the German Federal Ministry of Education and Research (BMBF) in the PEMPower project, grant number 03SF0771.

Data availability

The data supporting this article have been included as part of the ESI.†

Conflicts of interest

There are no conflicts to declare.

Notes and references

1 W. Fang, W. Guo, R. Lu, Y. Yan, X. Liu, D. Wu, F. M. Li, Y. Zhou, C. He, C. Xia, H. Niu, S. Wang, Y. Liu, Y. Mao, C. Zhang, B. You, Y. Pang, L. Duan, X. Yang, F. Song, T. Zhai, G. Wang, X. Guo, B. Tan, T. Yao, Z. Wang and B. Y. Xia, *Nature*, 2024, **626**, 86–91.
2 J. Wen, S. Tang, X. Ding, Y. Yin, F. Song and X. Yang, *Energies*, 2024, **17**, 5712.
3 X. Li, T. Ye, X. Meng, D. He, L. Li, K. Song, J. Jiang and C. Sun, *Polymers*, 2024, 16.
4 H. B. Tao, H. Liu, K. Lao, Y. Pan, Y. Tao, L. Wen and N. Zheng, *Nat. Nanotechnol.*, 2024, **19**, 1074–1076.
5 Q. Li, R. He, J. O. Jensen and N. J. Bjerrum, *Chem. Mater.*, 2003, **15**, 4896–4915.
6 G. Li, Y. Wang, F. Yu, Y. Lei and Z. Hu, *Chem. Commun.*, 2021, **57**, 4051–4054.
7 K. A. Page, K. M. Cable and R. B. Moore, *Macromolecules*, 2005, **38**, 6472–6484.
8 T. Kyu, M. Hashiyama and A. Eisenberg, *Can. J. Chem.*, 1983, **61**, 680–687.
9 M. Casciola, G. Alberti, M. Sganappa and R. Narducci, *J. Power Sources*, 2006, **162**, 141–145.
10 F. Arslan, K. Chuluunbandi, A. T. S. Freiberg, A. Kormanyos, F. Sit, S. Cherevko, J. Kerres, S. Thiele and T. Böhm, *ACS Appl. Mater. Interfaces*, 2021, **13**, 56584–56596.
11 R. Harilal, P. C. Nayak, P. C. Ghosh and T. Jana, *ACS Appl. Polym. Mater.*, 2020, **2**, 3161–3170.
12 G. Liu, H. Zhang, J. Hu, Y. Zhai, D. Xu and Z.-G. Shao, *J. Power Sources*, 2006, **162**, 547–552.
13 A. Kumar, *J. Mater. Chem. A*, 2020, **8**, 22632–22636.
14 K. Suzuki, Y. Iizuka, M. Tanaka and H. Kawakami, *J. Mater. Chem.*, 2012, **22**, 23767.
15 K. H. Lim, A. S. Lee, V. Atanasov, J. Kerres, E. J. Park, S. Adhikari, S. Maurya, L. D. Manriquez, J. Jung, C. Fujimoto, I. Matanovic, J. Jankovic, Z. Hu, H. Jia and Y. S. Kim, *Nat. Energy*, 2022, **7**, 248–259.
16 H. Huang, X. Zeng, X. Zhang and H. Li, *Energy Fuels*, 2023, **37**, 17516–17525.
17 T. Stigler, M. Wagner, S. Thiele and J. Kerres, *Macromolecules*, 2024, **57**, 364–372.
18 V. Atanasov and J. Kerres, *Macromolecules*, 2011, **44**, 6416–6423.
19 S. Auffarth, M. Wagner, A. Krieger, B. Fritsch, L. Hager, A. Hutzler, T. Böhm, S. Thiele and J. Kerres, *ACS Mater. Lett.*, 2023, **5**, 2039–2046.
20 G. Delaittre and L. Barner, *Polym. Chem.*, 2018, **9**, 2679–2684.
21 V. Atanasov, A. Oleynikov, J. Xia, S. Lyonnard and J. Kerres, *J. Power Sources*, 2017, **343**, 364–372.
22 S. Auffarth, M. Maier, P. Martschin, T. Stigler, M. Wagner, T. Böhm, A. Hutzler, S. Thiele and J. Kerres, *Mater. Today Adv.*, 2024, **23**, 100521.
23 T.-S. Chung, *Polym. Rev.*, 1997, **37**, 277–301.
24 C. Müller, *Chem. Mater.*, 2015, **27**, 2740–2754.
25 H.-C. Wu, C.-C. Hung, C.-W. Hong, H.-S. Sun, J.-T. Wang, G. Yamashita, T. Higashihara and W.-C. Chen, *Macromolecules*, 2016, **49**, 8540–8548.
26 S. E. Root, S. Savagatrup, A. D. Printz, D. Rodriquez and D. J. Lipomi, *Chem. Rev.*, 2017, **117**, 6467–6499.
27 T. J. Peckham and S. Holdcroft, *Adv. Mater.*, 2010, **22**, 4667–4690.
28 R. N. Haward, *J. Polym. Sci., Part A-2 Polym. Phys.*, 1969, **7**, 219–229.
29 N. Esmaeili, E. M. Gray and C. J. Webb, *ChemPhysChem*, 2019, **20**, 2016–2053.
30 M. Yamada, T. Sugihara and T. Yamada, *J. Electroanal. Chem.*, 2021, **897**, 115586.
31 A. Kumar, W. Pisula and K. Müllen, *Mater. Today Commun.*, 2019, **20**, 100539.
32 F. C. Teixeira, A. I. de Sá, A. P. S. Teixeira and C. M. Rangel, *New J. Chem.*, 2019, **43**, 15249–15257.
33 A. Kusoglu and A. Z. Weber, *Chem. Rev.*, 2017, **117**, 987–1104.
34 K.-D. Kreuer, *Chem. Mater.*, 1996, **8**, 610–641.
35 M. Vinothkannan, A. R. Kim, G. Gnana Kumar and D. J. Yoo, *RSC Adv.*, 2018, **8**, 7494–7508.